Cascade lasing at ~2 μm and ~2.3 μm in a diode-pumped Tm:YVO4 laser

Xiaoxu Yu, Zhognben Pan, Hongwei Chu, Fangyuan Zha, Han Pan, Lijuan Ma, Pavel Loiko, Patrice Camy, Dechun Li

Research Article | Vol. 31, No. 9 / 24 Apr 2023 / Optics Express 13576
Optics EXPRESS

Cascade lasing at ~2 μm and ~2.3 μm in a diode-pumped Tm:YVO_4 laser

Xiaoxu Yu,[1] Zhognben Pan,[1,3] Hongwei Chu,[1] Fangyuan Zha,[1] Han Pan,[1] Lijuan Ma,[1] Pavel Loiko,[2] Patrice Camy,[2] and Dechun Li[1,4]

[1]School of Information Science and Engineering, Shandong University, Qingdao 266237, China
[2]Centre de Recherche sur les Ions, les Matériaux et la Photonique (CIMAP), UMR 6252 CEA-CNRS-ENSICAEN, Université de Caen Normandie, 6 Boulevard Maréchal Juin, 14050 Caen Cedex 4, France
[3]zhongbenpan@sdu.edu.cn
[4]dechun@sdu.edu.cn

Abstract: We report on the cascade continuous-wave operation of a diode-pumped Tm:YVO_4 laser on the $^3F_4 \rightarrow {}^3H_6$ (at ~2 μm) and $^3H_4 \rightarrow {}^3H_5$ (at ~2.3 μm) Tm^{3+} transitions. Pumped with a fiber-coupled spatially multimode 794 nm AlGaAs laser diode, the 1.5 at.% Tm:YVO_4 laser yielded a maximum total output power of 6.09 W with a slope efficiency of 35.7% out of which the $^3H_4 \rightarrow {}^3H_5$ laser emission corresponded to 1.15 W at 2291-2295 and 2362-2371 nm with a slope efficiency of 7.9% and a laser threshold of 6.25 W.

1. Introduction

The development of application-oriented mid-infrared solid-state lasers is an important and hot research topic for the laser community. A simple and cost-efficient method to obtain laser emission in the short-wave infrared spectral range around 2.3 μm is to employ thulium lasers operating on the $^3H_4 \rightarrow {}^3H_5$ electronic transition [1], see Fig. 1 (a). In 1994, Pinto *et al.* reported on a Tm:$LiYF_4$ laser continuously tunable between 2.20 μm and 2.46 μm [2]. Thulium ions (Tm^{3+}) can be efficiently excited at 0.79 μm directly to the upper laser level ($^3H_4$), e.g., by commercially available high-power fiber-coupled AlGaAs laser diodes. Efficient and high-power Tm lasers operating on another transition, $^3F_4 \rightarrow {}^3H_6$ (at ~2 μm), have been realized by employing a variety of oxide and fluoride gain materials [3,4]. However, the power-scalable (multi-watt) continuous-wave (CW) operation of diode-pumped Tm lasers on the $^3H_4 \rightarrow {}^3H_5$ transition still remains a challenge. So far, the majority of results on ~2.3 μm Tm lasers, see, for example [5–7], were obtained under pumping by Ti:Sapphire lasers suffering from their complexity, high cost, and limited power scaling. Still, this approach allowed to prove the possibility of achieving high slope efficiencies from ~2.3 μm Tm lasers exceeding the Stokes limit: Guillemot presented a Tm:KY_3F_{10} laser generating 0.84 W at 2.34 μm by pumping at 773 nm, with a high slope efficiency of 47.7% (vs. the incident pump power) [5] owing to efficient energy-transfer upconversion (ETU, Fig. 1 (a)) leading to a pump quantum efficiency approaching 2 [8].

To date, diode-pumped CW laser operation of Tm lasers at ~2.3 μm has been realized only in a few Tm^{3+}-doped laser crystals, such as Tm:$Y_3Al_5O_{12}$ (Tm:YAG) [9], Tm:$YAlO_3$ (Tm:YAP) [9,10], and Tm:$LiYF_4$ (Tm:YLF) [9,11–14]. Kifle *et al.* presented a quasi-CW diode-pumped Tm:YAP laser delivering 2.69 W at 2.27 μm by pumping at 789 nm with a slope efficiency of 33.1% (vs. the absorbed pump power) and a laser threshold of 4.53 W [9].

Among the laser host materials for Tm^{3+} doping with the goal of developing diode-pumped lasers, yttrium orthovanadate (YVO_4) is attracting attention [15–17]. This crystal is tetragonal (sp. gr. $I4_1/amd$) and optically uniaxial (positive). YVO_4 can be grown by the conventional Czochralski method. As a host matrix, it offers high thermal conductivity (8.9 $Wm^{-1}K^{-1}$ and

#484647 https://doi.org/10.1364/OE.484647
Journal © 2023 Received 10 Jan 2023; revised 16 Mar 2023; accepted 18 Mar 2023; published 11 Apr 2023

Optics EXPRESS

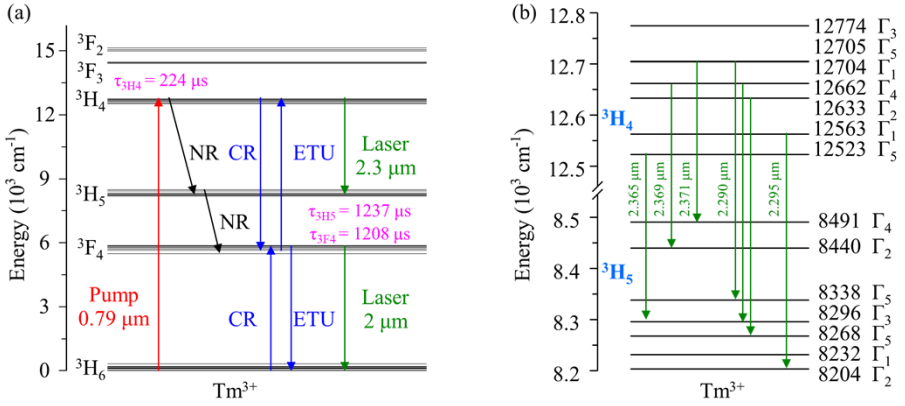

Fig. 1. (a) Partial energy level scheme of Tm^{3+} in YVO_4: *red and green arrows*, pump and laser transitions, respectively; *black arrows*, non-radiative (NR) relaxation; *blue arrows*, cross-relaxation (CR) and energy-transfer upconversion (ETU) processes; τ_{3H4}, τ_{3H5} and τ_{3F4}, luminescence lifetimes of the $^3H_4$, $^3H_5$, and $^3F_4$ states for 5 at.% Tm:YVO_4, respectively [16]; (b) crystal-field splitting of the $^3H_4$ and $^3H_5$ multiplets, Γ_i (i = 1-5), irreducible representations for the Stark sub-levels, D_{2d} site symmetry (after [15,21]), *green arrows*, observed laser lines.

12.1 $Wm^{-1}K^{-1}$ along the ***a*** and ***c*** axes, respectively) [18], weak anisotropy of thermal expansion, and positive thermo-optic coefficients [19] resulting in the positive thermal lens which is essential for microchip laser operation [20]. Tm^{3+} ions in the YVO_4 crystal feature a relatively broad $^3H_6 \rightarrow {}^3H_4$ absorption band which is advantageous for diode-pumping due to a weak sensitivity to the possible temperature drift of the diode wavelength, as well as polarized emission at ~2 μm [16].

Dual-waveband lasers simultaneously emitting at ~2 μm and ~2.3 μm based on a single gain medium appear promising for several applications fields. (i) The ~2 μm emission spectrally matches a strong absorption band of water and is relatively eye-safe, being relevant for clinical medical treatment [22–24]. The ~2.3 μm emission is weakly absorbed by water while overlaps with a characteristic absorption band of glucose ($C_6H_{12}O_6$), being very suitable for non-invasive glucose blood measurement [25,26]. In some surgeries such as cardiovascular surgery [27], insulinoma resection [28], cardiac surgery [29,30], and liver transplantation surgery [31], real-time continuous non-invasive glucose blood monitoring is essential. Especially for diabetic patients, such monitoring can greatly reduce the risk. (ii) The ~2 μm and ~2.3 μm emissions are located in the atmospheric transparency windows and are suitable for free-space telecommunications, laser imaging radar, and range-finding. The simultaneous dual-waveband operation of a laser could facilitate the expansion of information propagation capability by increasing the number of channels and could enhance the measurement accuracy as a result of double detection [32]. (iii) The ~2 μm emission overlaps with strong absorption bands of water vapor and CO_2 and a weak absorption band of CO, while the ~2.3 μm one matches with the weak absorption bands of water vapor and CO_2 [33] and strong absorption bands of CO, N_2O, CH_4, C_2H_2, and N_2O. The detection of multiple gas components can be realized simultaneously by a single simultaneous dual-waveband laser operating at ~2 μm and ~2.3 μm. Therefore, the availability of dual-waveband ~2 μm and ~2.3 μm sources can provide greater flexibility, convenience, and selectivity for the above-mentioned applications. Cascade lasing on two transitions can also decrease the overall quantum defect [34].

In the present work, we aimed to demonstrate the first dual-waveband laser operation at ~2 μm and ~2.3 μm of a diode-pumped Tm:YVO_4 laser based on cascade lasing on the $^3F_4 \rightarrow {}^3H_6$ and $^3H_4 \rightarrow {}^3H_5$ Tm^{3+} transitions. Multiple laser lines were observed around 1.95 μm, 2.29 μm,

Optics EXPRESS

and 2.36 µm, overlapping with strong absorption bands of gas molecules H_2O and CO_2 (~1.95 µm), N_2O (~2.28 µm), CO (~2.36 µm), and CH_4 (~2.37 µm), indicating a great potential of such lasers for atmospheric environmental monitoring.

2. Laser set-up

As a gain material, we have employed Tm:YVO_4. Two doping levels of 1.5 at.% and 3.0 at.% Tm^{3+} were tested. The crystals were grown by the Czochralski method. Rectangular laser elements were oriented for light propagation along the ***a*** crystallographic axis (***a***-cut) having a thickness of 10 mm and an aperture of 3.0×3.0 mm^2. Both their end faces were polished to laser-grade quality and antireflection (AR) coated for 0.79 ± 0.01 µm (reflectance: $R < 0.5\%$) and 1.85-2.36 µm ($R < 1\%$). Figure 2 (a) shows the schematic of the laser set-up. A simple compact plano-plano laser cavity was employed with a geometrical length of 13 mm. It was formed by a flat input mirror (M_1) coated for high transmission at 0.79 µm and high reflection at 1.8-2.4 µm and two different flat output mirrors supporting laser operation on two Tm^{3+} laser transitions of interest (M_2): one providing a transmission T_{OC} of 2% at 1.8-2.1 µm and 1% at 2.1-2.4 µm (labelled: OC_1) and another one-T_{OC} of 5% at 1.8-2.1 µm and 2% at 2.1-2.4 µm (labelled: OC_2). The Tm:YVO_4 crystal was wrapped with indium foil and mounted in a water-cooled copper block with a temperature set at 12 °C. The crystal was placed close to the input mirror. The pump source was a ~794 nm fiber-coupled AlGaAs laser diode (fiber core diameter: 200 µm, numerical aperture (N.A.): 0.22). The pump beam was collimated and focused into the laser crystal through the input mirror using a 1:1 collimation system (focal length: $f = 50$ mm) resulting in a waist diameter of 200 µm. The residual pump was filtered out using a long-pass filter (F_1) with a cutoff wavelength of 1 µm. Another long-pass filter (F_2) with a transmission of ~90% at ~2.3 µm and almost zero transmission at ~2 µm was used to separate the ~2.3 µm power contribution. The laser emission spectra were measured using an optical spectrum analyzer (APE GmbH, Germany).

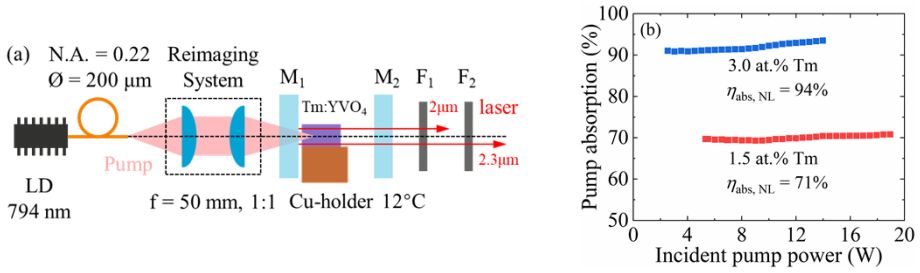

Fig. 2. (a) Scheme of the diode-pumped Tm:YVO_4 laser: LD-laser diode, M_1-input mirror, M_2-output coupler, F_1 and F_2-long-pass (LP) filters; (b) pump absorption under non-lasing conditions as a function of the incident pump power.

Even though the high reflections were provided by both studied output couplers at 794 nm, the back-reflected divergent pump makes little contribution to the gain. Thus, the pumping was in single pass. The pump absorption efficiency under non-lasing conditions $\eta_{abs,NL}$ for both Tm:YVO_4 crystals was initially determined in pump-transmission measurements [35]. The $\eta_{abs,NL}$ as a function of the incident pump power is plotted in Fig. 2 (b). It was weakly dependent on the pump level indicating almost negligible bleaching of the ground state and amounted to 71% (1.5 at.% Tm) and 94% (3.0 at.% Tm). Subsequently, the pump absorption efficiency under lasing conditions was estimated from the $\eta_{abs,NL}$ value at the threshold pump power.

Optics EXPRESS

3. Results and discussion

First, we studied the laser performance of the 1.5 at.% Tm:YVO_4 crystal using both output couplers (OC_1 and OC_2), see Fig. 3 (a, b). Here, we use the following notations: P_Σ-the total output power, $P_\Sigma = P_{2}\mu m + P_{2.3}\mu m$, where $P_{2}\mu m$ and $P_{2.3}\mu m$ are the output powers for the $^3F_4 \rightarrow {}^3H_6$ and $^3H_4 \rightarrow {}^3H_5$ Tm^{3+} transitions, respectively, and η_Σ ($\eta_{2}\mu m$ and $\eta_{2.3}\mu m$) are the corresponding laser slope efficiencies vs. the pump power absorbed in the laser crystal. and $P_{th,2}\mu m$ and $P_{th,2.3}\mu m$ denote the laser thresholds for both transitions. We also define the power fraction of the laser emission on the $^3H_4 \rightarrow {}^3H_5$ Tm^{3+} transition, $X = P_{2.3}\mu m/P_\Sigma$.

The laser operation in the plano-plano cavity was ensured by the positive (focusing) thermal lens of the Tm:YVO_4 crystal arising from a positive thermo-optic coefficient dn/dT of this material [19].

The output characteristics of the Tm:YVO_4 laser are summarized in Table 1.

Table 1. Output Performance[a] of CW Cascade Diode-Pumped Tm:YVO_4 Lasers

Crystal	M_2	Total output		$^3F_4 \rightarrow {}^3H_6$ transition			$^3H_4 \rightarrow {}^3H_5$ transition		
		P_Σ, W	η_Σ, %	$P_{2}\mu m$, W	$P_{th,2}\mu m$, W	$\eta_{2}\mu m$, %	$P_{2.3}\mu m$, W	$P_{th,2.3}\mu m$, W	$\eta_{2.3}\mu m$, %
1.5 at.% Tm:YVO_4	OC_1	4.47	32.0	3.37	3.72	23.4	1.10	5.08	9.0
	OC_2	6.09	35.7	4.94	4.81	28.1	1.15	6.25	7.9
3.0 at.% Tm:YVO_4	OC_1	2.16	27.1	1.60	4.96	20.3	0.56	4.96	7.1
	OC_2	-	-	0.66	9.17	27.3	-	-	-

[a]M_2, output coupler; P, the maximum output power; η, laser slope efficiency vs. the absorbed pump power; P_{th}, laser threshold..

Higher total output power, as well as that for the $^3H_4 \rightarrow {}^3H_5$ Tm^{3+} transition, were achieved when using higher output coupling (OC_2, $T_{OC} = 5\%/2\%$), see Fig. 3 (b). For the maximum absorbed pump power of 22.24 W, the 1.5 at.% Tm:YVO_4 laser generated a maximum total output power P_Σ of 6.09 W with a slope efficiency η_Σ of 35.7% and a laser threshold $P_{th,2}\mu m$ of 4.81 W. The optical efficiency reached 27.4%. The emission on the $^3F_4 \rightarrow {}^3H_6$ transition corresponded to higher output power ($P_{2}\mu m = 4.94$ W), higher slope efficiency ($\eta_{2}\mu m = 28.1\%$), and lower laser threshold, i.e., first, only the emission at ~2 μm appeared and for pump powers exceeding $P_{th,2.3}\mu m$ of 6.25 W, both $^3F_4 \rightarrow {}^3H_6$ and $^3H_4 \rightarrow {}^3H_5$ laser emissions were observed, and the two laser emissions were time-domain synchronized. For Tm lasers operating on the $^3H_4 \rightarrow {}^3H_5$ transition with a direct pumping to the upper laser level ($^3H_4$), the characteristic laser establishment time (i.e., the time interval between switching on the pump and the first laser oscillations) is faster than 1 ms [36]. The highest $P_{2.3}\mu m$ reached 1.15 W with a slope efficiency $\eta_{2.3}\mu m$ of 7.9%. The input-output dependences for both the total output power and the power contributions on both laser transitions were linear within the studied range of pump powers, further power scaling was limited by the available pump power.

A similar behavior was observed for smaller output coupling (OC_1, $T_{OC} = 2\%/1\%$), as shown in Fig. 3 (a). For the maximum absorbed pump power of 17.63 W, the maximum total output power P_Σ was 4.47 W with a slope efficiency η_Σ of 32.0% and a laser threshold $P_{th,2}\mu m$ of 3.72 W. The optical efficiency was 25.4%. For the $^3H_4 \rightarrow {}^3H_5$ transition, the laser generated an output power $P_{2.3}\mu m$ of 1.10 W with a higher slope efficiency $\eta_{2.3}\mu m$ of 9.0% and a lower laser threshold $P_{th,2.3}\mu m$ of 5.08 W (as compared to OC_2). More details can be found in Table 1.

For the 3.0 at.% Tm:YVO_4 crystal, the laser performance deteriorated, see Fig. 3 (c). Cascade lasing was achieved only for small output coupling (OC_1). For the maximum absorbed pump power of 13.08 W, the maximum total output power P_Σ of the cascade laser was 2.16 W with a slope efficiency η_Σ of 27.1% and a laser threshold $P_{th,2}\mu m$ of 4.96 W. The optical efficiency was 16.5%. For the $^3H_4 \rightarrow {}^3H_5$ transition, the corresponding output power $P_{2.3}\mu m$ reached

Optics EXPRESS

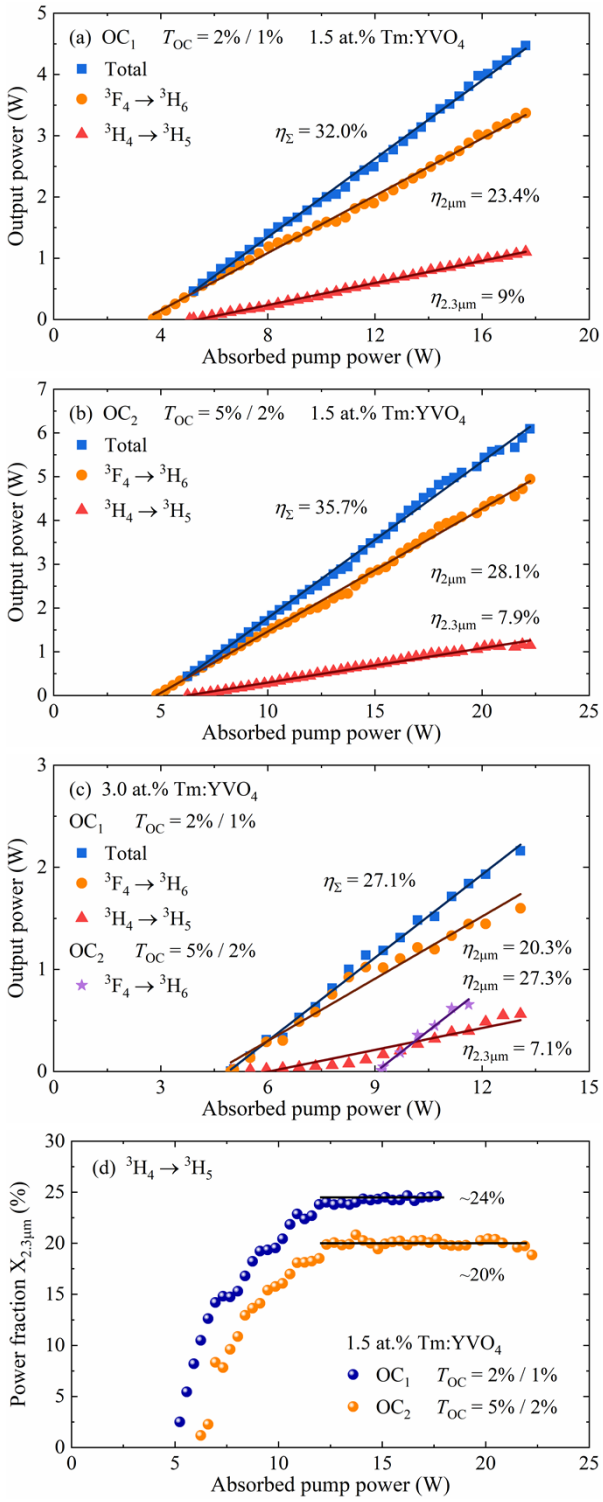

Fig. 3. Diode-pumped cascade Tm:YVO_4 lasers simultaneously operating on the $^3F_4 \rightarrow {}^3H_6$ and $^3H_4 \rightarrow {}^3H_5$ transitions: (a-c) input-output dependences, η-slope efficiency: (a, b) the 1.5 at.% Tm:YVO_4 crystal, output couplers: (a) OC_1 and (b) OC_2; (c) the 3.0 at.% Tm:YVO_4 crystal with both OC_1 and OC_2; (d) power fraction X of the $^3H_4 \rightarrow {}^3H_5$ emission.

Optics EXPRESS

0.56 W with a slope efficiency $\eta_{2.3\mu m}$ of 7.1% and a laser threshold $P_{th,2.3\mu m}$ of 4.96 W. For a Tm^{3+} dopant concentration greater than 2 at.%, the $^3H_4$ manifold fluorescence lifetime will be significantly quenched by the CR process, which is favorable for the $^3F_4 \rightarrow {}^3H_6$ Tm^{3+} transition but unfavorable for the $^3H_4 \rightarrow {}^3H_5$ one. Therefore, the deteriorated laser performance of the heavily doped 3.0 at.% Tm:YVO_4 crystal is probably due to the stronger competition between the high-gain $^3F_4 \rightarrow {}^3H_6$ transition and the low-gain $^3H_4 \rightarrow {}^3H_5$ one. For higher output coupling (OC_2), the laser operated solely on the $^3F_4 \rightarrow {}^3H_6$ transition, as we were unable to reach the second laser threshold for the $^3H_4 \rightarrow {}^3H_5$ transition.

The power fraction of the $^3H_4 \rightarrow {}^3H_5$ laser emission as a function of absorbed pump power is plotted in Fig. 3 (d) for the two studied output couplers. It rapidly increases above the laser threshold $P_{th,2.3\mu m}$ and saturates for pump levels well exceeding the threshold pump power, reaching X about 24% (OC_1) and 20% (OC_2).

The typical spectra of cascade laser emission achieved with two output couplers and the 1.5 at.% Tm:YVO_4 crystal are shown in Fig. 4 (a, b). Here, the spectral intensities for the two observed laser transitions were normalized for better visibility, while the corresponding output powers can be seen in Fig. 3 (a, b). The spectra were measured at different absorbed pump powers.

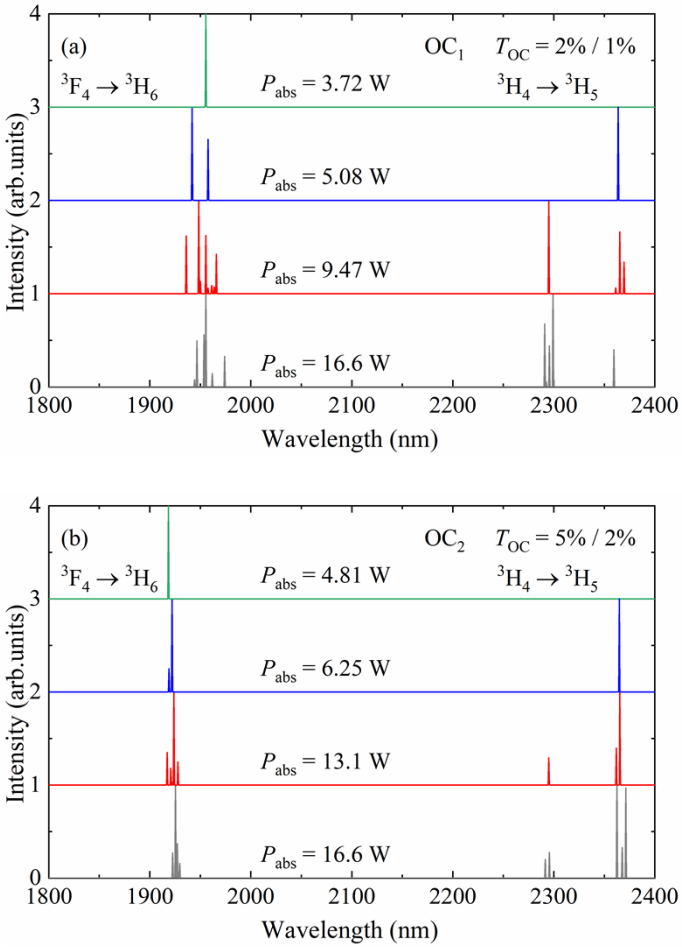

Fig. 4. The spectra of output emission from the diode-pumped cascade 1.5 at.% Tm:YVO_4 laser captured at different absorbed pump powers P_{abs}: (a) OC_1 and (b) OC_2.

Optics EXPRESS

Table 2 summarizes the observed laser wavelengths (as the main focus of the present work is the $^3H_4 \rightarrow {}^3H_5$ Tm^{3+} transition, exact values for each laser line are given while for the $^3F_4 \rightarrow {}^3H_6$ transition, only the spectral range is indicated).

Table 2. Laser Wavelengths of the Cascade Diode-Pumped Tm:YVO_4 Laser at Different Pump Powers

P_{abs}, W	OC_1: λ_L, nm		P_{abs}, W	OC_2: λ_L, nm	
	$^3F_4 \rightarrow {}^3H_6$	$^3H_4 \rightarrow {}^3H_5$		$^3F_4 \rightarrow {}^3H_6$	$^3H_4 \rightarrow {}^3H_5$
3.72	1955	-	4.81	1918	-
5.08	1941, 1957	2363	6.25	1919, 1921	2364
9.47	1936-1965	2295, 2361, 2365, 2369	13.1	1917-1927	2295, 2361, 2365
16.6	1944-1974	2290, 2292, 2295, 2299, 2359	16.6	1922-1929	2291, 2295, 2362, 2367, 2371

For the $^3F_4 \rightarrow {}^3H_6$ Tm^{3+} transition, with increasing the output couplers (from 2% for OC_1 to 5% for OC_2), the laser wavelength experienced a noticeable blue-shift, from 1944-1974nm to 1922-1929nm at the absorbed pump power of 16.6 W. This behavior is typical for quasi-three-level laser transitions with inherent reabsorption at the emission wavelength and is related to decreasing reabsorption losses at higher inversion in the gain medium associated with the higher transmission of the output coupler [16]. It also agrees with the gain spectra of Tm^{3+} in the YVO_4 crystal [15]. At the threshold pump power, the laser operated on a single line (1955nm/1918nm for OC_1/OC_2, respectively). With increasing the pump power, multiple longitudinal laser modes were generated. They are due to the etalon effect at the air gap between the input mirror M_1 and the laser crystal, as well as the relatively broad gain spectra of Tm^{3+}. This was verified by varying the pump power, which, due to the positive thermal expansion of the crystal in the longitudinal direction, affected the laser spectra.

For the quasi-four-level $^3H_4 \rightarrow {}^3H_5$ Tm^{3+} transition, as expected, the spectral position of the laser lines was almost independent of the output couplers. For OC_1 and OC_2, at the threshold pump powers, the laser operated at single lines of 2363 nm and 2364 nm, respectively. With increasing the pump power, multiple laser lines appeared within two spectral ranges, at ~2.29 μm and ~2.36 μm, cf. Table 2. The mechanism of appearance of these lines is similar to that for the $^3F_4 \rightarrow {}^3H_6$ Tm^{3+} transition.

Cascade laser emission from rare-earth ions provides a dual-waveband output with a large wavelength separation, which can help to simultaneously address different applications (see the Introduction section). In our case, well above the laser thresholds for both Tm^{3+} laser transitions, the ratio between the corresponding power components $P_{2.3\mu m}/P_{2\mu m}$ was almost constant (a non-competitive laser operation).

Simultaneous laser operation of Tm^{3+} on the $^3H_4 \rightarrow {}^3H_5$ and $^3F_4 \rightarrow {}^3H_6$ transitions is a bit different from cascade lasing of Er^{3+} [37] or Ho^{3+} [38] where an intermediate metastable level $|1>$ plays two roles: a terminal laser level for a transition from a higher-lying excited-state $|2> \rightarrow |1>$ and an emitting level for a transition to the ground-state $|1> \rightarrow |0>$. By allowing the simultaneous operation on both transitions, the metastable level $|1>$ can be fast depopulated avoiding the bottleneck effect. In our case, the efficient multiphonon non-radiative relaxation from the $^3H_5$ Tm^{3+} state (the terminal laser level for the $^3H_4 \rightarrow {}^3H_5$ transition) naturally helps to avoid the bottleneck effect. However, the long lifetime of the $^3F_4$ Tm^{3+} state may play a significant role, especially at high pump intensities by accumulating the electronic excitations in this manifold and causing a non-negligible ground-state bleaching thus reducing the pump absorption efficiency. Cascade lasing can remove this limitation.

Huang *et al.* reported on cascade lasing from a diode-pumped Tm:$LiYF_4$ laser delivering a maximum total output power of 5.49 W of which 1.12 W was generated at 2305 nm with a

Optics EXPRESS

slope efficiency of ~8.6% [34]. Obviously, Tm:YVO_4 allows to access longer wavelengths of the mid-infrared emission.

4. Conclusions

To conclude, Tm:YVO_4 is a promising crystal for efficient, multi-watt CW diode-pumped lasers simultaneously emitting at ~2 μm and ~2.3 μm due to a cascade laser scheme, $^3H_4 \rightarrow {}^3H_5$ and $^3F_4 \rightarrow {}^3H_6$. We report on a non-competitive (in terms of the relative power fractions) cascade laser operation of a diode-pumped 1.5 at.% Tm:YVO_4 laser delivering a total output power of >6 W at ~1.95 μm, ~2.29 μm, and ~2.36 μm with a high slope efficiency of 35.7% out of which the mid-infrared laser emission owing to the $^3H_4 \rightarrow {}^3H_5$ transition corresponded to 1.15 W with a slope efficiency of 7.9% and a laser threshold of 6.25 W. We also analyzed the effect of the output coupling and Tm^{3+} doping level on the dual-waveband laser operation. Simultaneous dual-waveband laser sources emitting at ~2 μm and ~2.3 μm based on a single laser medium are attractive for applications in cardiovascular surgery, free-space telecommunications, and gas composition detection.

Funding. National Natural Science Foundation of China (52072351, 12004213, 12174223, 12274263, 21872084, 62175128); "RELANCE" Chair of Excellence project funded by the Normandy Region; Qilu Young Scholar Program of Shandong University.

Disclosures. The authors declare no conflicts of interest.

Data availability. Data underlying the results presented in this paper are not publicly available at this time but may be obtained from the authors upon reasonable request.

References

1. J. A. Caird, L. G. DeShazer, and J. Nella, "Characteristics of room-temperature 2.3-μm laser emission from Tm^{3+} in YAG and $YAlO_3$," IEEE J. Quantum Electron. **11**(11), 874–881 (1975).
2. J. F. Pinto, L. Esterowitz, and G. H. Rosenblatt, "Tm^{3+}:YLF laser continuously tunable between 2.20 and 2.46 μm," Opt. Lett. **19**(12), 883–885 (1994).
3. M. Schellhorn, "High-power diode-pumped Tm:YLF laser," Appl. Phys. B **91**(1), 71–74 (2008).
4. E. C. Honea, R. J. Beach, S. B. Sutton, J. A. Speth, S. C. Mitchell, J. A. Skidmore, M. A. Emanuel, and S. A. Payne, "115-W Tm:YAG diode-pumped solid-state laser," IEEE J. Quantum Electron. **33**(9), 1592–1600 (1997).
5. L. Guillemot, P. Loiko, R. Soulard, A. Braud, J.-L. Doualan, A. Hideur, and P. Camy, "Close look on cubic Tm:KY_3F_{10} crystal for highly efficient lasing on the $^3H_4 \rightarrow {}^3H_5$ transition," Opt. Express **28**(3), 3451–3463 (2020).
6. P. Loiko, E. Kifle, L. Guillemot, J.-L. Doualan, F. Starecki, A. Braud, M. Aguiló, F. Díaz, V. Petrov, X. Mateos, and P. Camy, "Highly efficient 2.3 μm thulium lasers based on a high-phonon-energy crystal: evidence of vibronic-assisted emissions," J. Opt. Soc. Am. B **38**(2), 482–495 (2021).
7. F. Canbaz, I. Yorulmaz, and A. Sennaroglu, "Kerr-lens mode-locked 2.3-μm Tm^{3+}:YLF laser as a source of femtosecond pulses in the mid-infrared," Opt. Lett. **42**(19), 3964–3967 (2017).
8. P. Loiko, R. Soulard, L. Guillemot, G. Brasse, J.-L. Doulan, A. Braud, A. Tyazhev, A. Hideur, F. Druon, and P. Camy, "Efficient Tm:$LiYF_4$ lasers at ~2.3 μm: Effect of energy-transfer upconversion," IEEE J. Quantum Electron. **55**(6), 1–12 (2019).
9. E. Kifle, P. Loiko, L. Guillemot, J.-L. Doualan, F. Starecki, A. Braud, T. Georges, J. Rouvillain, and P. Camy, "Watt-level diode-pumped thulium lasers around 2.3 μm," Appl. Optics **59**(25), 7530–7539 (2020).
10. F. Wang, H. Huang, F. Wu, H. Chen, Y. Bao, Z. Li, O. L. Antipov, S. S. Balabanov, and D. Shen, "2.3-2.5 μm laser operation of LD-pumped Tm:YAP on the $^3H_4 \rightarrow {}^3H_5$ transition," Opt. Mater. **115**, 111054 (2021).
11. I. Yorulmaz and A. Sennaroglu, "Low-threshold diode-pumped 2.3-μm Tm^{3+}:YLF lasers," IEEE J. Sel. Top. Quantum Electron. **24**(5), 1–7 (2018).
12. S. Wang, H. Huang, H. Chen, X. Liu, S. Liu, J. Xu, and D. Shen, "High efficiency nanosecond passively Q-switched 2.3 μm Tm:YLF laser using a $ReSe_2$-based saturable output coupler," OSA Continuum **2**(5), 1676–1682 (2019).
13. Y. Zhang, Y. Cai, B. Xu, Y. Yang, and Y. Hang, "Extending the wavelength tunability from 2.01 to 2.1 μm and simultaneous dual-wavelength operation at 2.05 and 2.3 μm in diode-pumped Tm:YLF lasers," J. Lumin. **218**, 116873 (2020).
14. F. Wang, H. Huang, H. Chen, Y. Bao, Z. Li, and D. Shen, "GSA and ESA dual-wavelength pumped 2.3 μm Tm:YLF laser on the $^3H_4 \rightarrow {}^3H_5$ transition," Chin. Opt. Lett. **19**(9), 091405 (2021).
15. R. Lisiecki, P. Solarz, G. Dominiak-Dzik, W. Ryba-Romanowski, M. Sobczyk, P. Černý, J. Šulc, H. Jelínková, Y. Urata, and M. Higuchi, "Comparative optical study of thulium-doped YVO_4, $GdVO_4$, and $LuVO_4$ single crystals," Phys. Rev. B **74**(3), 035103 (2006).
16. K. Ohta, H. Saito, and M. Obara, "Spectroscopic characterization of Tm^{3+}:YVO_4 crystal as an efficient diode pumped laser source near 2000nm," J. Appl. Phys. **73**(7), 3149–3152 (1993).

Optics EXPRESS

17. X. Yu, H. Chu, F. Zha, H. Pan, S. Zhao, Z. Pan, and D. Li, "Watt-level diode-pumped Tm:YVO_4 laser at 2.3 μm," Opt. Lett. **47**(21), 5501–5504 (2022).
18. Y. Sato and T. Taira, "The studies of thermal conductivity in $GdVO_4$, YVO_4, and $Y_3Al_5O_{12}$ measured by quasi-one-dimensional flash method," Opt. Express **14**(22), 10528–10536 (2006).
19. P. A. Loiko, K. V. Yumashev, V. N. Matrosov, and N. V. Kuleshov, "Dispersion and anisotropy of thermo-optic coefficients in tetragonal $GdVO_4$ and YVO_4 laser host crystals: erratum," Appl. Opt. **54**(15), 4820–4822 (2015).
20. G. L. Bourdet and G. Lescroart, "Theoretical modelling and design of a Tm:YVO_4 microchip laser," Opt. Commun. **149**(4-6), 404–414 (1998).
21. D. E. Wortman, R. P. Leavitt, and C. A. Morrison, "Analysis of the ground configuration of Tm^{3+} in YVO_4," J. Phys. Chem. **35**(4), 591–593 (1974).
22. T. Bach, T. R. W. Herrmann, C. Cellarius, and A. J. Gross, "Bladder neck incision using a 70 W 2 micron continuous wave laser (RevoLix)," World J. Urol. **25**(3), 263–267 (2007).
23. C. Zhong, S. Guo, Y. Tang, and S. Xia, "Clinical observation on 2 micron laser for non-muscle-invasive bladder tumor treatment: single-center experience," World J. Urol. **28**(2), 157–161 (2010).
24. Z. Yao, B. Sun, G. Zhou, Y. Yang, L. Zhang, L. Liu, H. Sheng, and H. Guo, "Application of two micron laser vaporesection combined with transurethral resection of the prostate in treatment of benign prostatic hyperplasia: analysis of 340 cases," Int. J. Clin. Exp. Med. **8**(10), 19418–19423 (2015).
25. S. T. Fard, W. Hofmann, P. T. Fard, G. Böhm, M. Ortsiefer, E. Kwok, M. C. Amann, and L. Chrostowski, "Optical absorption glucose measurements using 2.3 μm vertical-cavity semiconductor lasers," IEEE Photonics Technol. Lett. **20**(11), 930–932 (2008).
26. J. T. Olesberg, M. A. Arnold, C. Mermelstein, J. Schmitz, and J. Wagner, "Tunable laser diode system for noninvasive blood glucose measurements," Appl. Spectrosc. **59**(12), 1480–1484 (2005).
27. K. Kawahito, H. Sato, M. Kadosaki, A. Egawa, and Y. Misawa, "Spike in glucose levels after reperfusion during aortic surgery: assessment by continuous blood glucose monitoring using artificial endocrine pancreas," Gen. Thorac. **66**(3), 150–154 (2018).
28. Y. Sugiyama, C. Kiuchi, M. Suzuki, Y. Maruyama, R. Wakabayashi, Y. Ohno, S. Takahata, T. Shibazaki, and M. Kawamata, "Glucose management during insulinoma resection using real-time subcutaneous continuous glucose monitoring," Case reports in anesthesiology **2018**, 1–4 (2018).
29. H. G. Piper, J. L. Alexander, A. Shukla, F. Pigula, J. M. Costello, P. C. Laussen, T. Jaksic, and M. S. D. Agus, "Real-time continuous glucose monitoring in pediatric patients during and after cardiac surgery," Pediatrics **118**(3), 1176–1184 (2006).
30. B. Kalmovich, Y. Bar-Dayan, M. Boaz, and J. Wainstein, "Continuous glucose monitoring in patients undergoing cardiac surgery," Diabetes Technol. Ther. **14**(3), 232–238 (2012).
31. T. Okada, S. Kawahito, N. Mita, M. Matsuhisa, H. Kitahata, M. Shimada, and S. Oshita, "Usefulness of continuous blood glucose monitoring and control for patients undergoing liver transplantation," J. Med. Investig. **60**(3.4), 205–212 (2013).
32. J. Li, H. Luo, L. Wang, Y. Liu, Z. Yan, K. Zhou, L. Zhang, and S. K. Turistsyn, "Mid-infrared passively switched pulsed dual wavelength Ho^{3+}-doped fluoride fiber laser at 3 μm and 2 μm," Sci. Rep. **5**(1), 10770 (2015).
33. M. E. Webber, J. Wang, S. T. Sanders, D. S. Baer, and R. K. Hanson, "In situ combustion measurements of CO, CO_2, H_2O and temperature using diode laser absorption sensors," Proc. Combust. Inst. **28**(1), 407–413 (2000).
34. H. Huang, S. Wang, H. Chen, O. L. Antipov, S. S. Balabanov, and D. Shen, "High power simultaneous dual-wavelength CW and passively-Q-switched laser operation of LD pumped Tm:YLF at 1.9 and 2.3 μm," Opt. Express **27**(26), 38593–38601 (2019).
35. F. Zha, X. Yu, H. Chu, H. Pan, S. Zhao, P. Loiko, Z. Pan, and D. Li, "Compact diode-pumped continuous wave and passively Q switched Tm:YAG laser at 2.33 μm," Opt. Lett. **47**(23), 6265–6268 (2022).
36. L. Guillemot, P. Loiko, R. Soulard, A. Braud, J.-L. Doualan, A. Hideur, R. Moncorge, and P. Camy, "Thulium laser at ~2.3 μm based on upconversion pumping," Opt. Lett. **44**(16), 4071–4074 (2019).
37. B. Schmaul, G. Huber, R. Clausen, B. Chai, P. LiKamWa, and M. Bass, "Er^{3+}:$YLiF_4$ continuous wave cascade laser operation at 1620 and 2810 nm at room temperature," Appl. Phys. Lett. **62**(6), 541–543 (1993).
38. S. Ye, X. Zhou, S. Huang, H. Nie, J. Bian, T. Li, K. Yang, J. He, and B. Zhang, "Cascade MIR Ho:YLF laser at 2.1 μm and 2.9 μm," Opt. Lett. **47**(21), 5642–5645 (2022).